DC Load Flow Models for the Electric Power System of Wide Body All Electric Aircraft

Mona Ghassemi, Ashkan Barzkar
Bradley Department of Electrical and Computer Engineering, Virginia Tech
Blacksburg, VA 24061, USA
monag@vt.edu, barzkar@vt.edu

***Abstract*—In this paper, a novel bipolar ±5 kV medium voltage direct current (MVDC) electric power system (EPS) having a distributed propulsion architecture is proposed to make the envisaged turboelectric NASA N3-X become all electric aircraft (AEA). Dimensions of the aircraft are estimated, and potential conductors for different cables connecting different buses are selected. Power flow (PF) analysis is done for the proposed EPS regarding selected conductors and calculated resistances, and results are discussed. To perform the PF analysis, since the target network is a DC network, a PF for DC power systems based on monotone mapping is developed and adapted to analyze the proposed all electric N3-X aircraft EPS. It is shown that the EPS proposed is reliable both in normal condition and all n-1 contingency situations, even when losing a busbar.**

TABLE OF CONTENTS

1. INTRODUCTION

Wide-body aircraft are responsible for 33% of aviation greenhouse gas emissions, where the situation becomes worse when considering more than 4% annual growth in air travel [1]. Also, 2019 was the second warmest year on record. A promising solution to combat greenhouse gas emissions and global warming is transportation electrification. Electrification has given birth to more electric aircraft (MEA) and all electric aircraft (AEA) in the aviation industry. Even though the benefits mentioned for MEA and AEA are overstatements in some publications, many advantages are recognized and discussed for electrified aircraft in the literature [1-3].

There are four main types of energies in conventional aircraft: electrical, mechanical, hydraulic, and pneumatic. An MEA can be achieved by simply replacing a non-electrical subsystem with its electrical alternative while attaining an AEA is challenging. In AEA, not only all systems/subsystems are required to be replaced by their electrical alternatives, but the propulsion power must also be provided electrically. As shown in Figure 1, in conventional aircraft such as the Boeing 707 and the Boeing 737, less than 100 kVA electrical power is found, while 1 MVA electrical power is found within the MEA Boeing 787. This 1 MVA is except for the auxiliary power unit (APU) which itself provides 0.45 MVA electrical power. However, if all non-propulsive loads are considered, less than 5 MW electrical power is consumed, while at least 25-30 MW power is required in wide-body aircraft during take-off that must be provided by electrochemical energy units (EEU) in AEA.

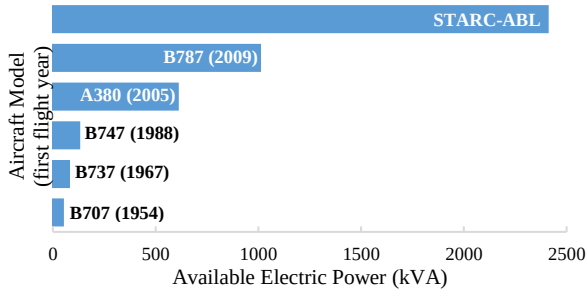

Figure 1. Aircraft models (first flight year) vs. available electric power. A380, B787, and STARC-ABL are MEA. STARC-ABL is not commercially available.

Using today's technologies, this immense amount of power is out of reach [4]; however, research activities sponsored by governmental and private entities have been done and targeted to achieve this. On the other hand, other electrical propulsion architectures were introduced and designed for electrified aircraft, such as the turboelectric NASA N3-X aircraft [5]. In the NASA design, the power extracted from engines is turned into electrical energy and is distributed electrically to supply fourteen distributed motors. Also, as will be discussed in this paper, hybrid electric structures are possible.

The trend is to employ DC networks for electrified aircraft to pave the way for aircraft EPS optimization. However, motivated by Paschen's law and the very low-pressure condition that aircraft undergoes during a flight, today's highest DC-employed voltage is 540 V_{DC} (±270 V_{DC}) [6]. However, an increase in DC voltage level reduces the mass of the system. For instance, elevating voltage level from 540 V_{DC} to 4.8 kV_{DC} results in 1.4 tones of cable conductor mass

978-1-6654-3760-8/22/$31.00 ©2022 IEEE

saving for NASA STARC-ABL [7]; in addition, NASA proposed a ±2 kV_{DC} for N3-X aircraft [8]. Therefore, there is a clear trend toward MVDC networks in the aviation industry, and it is crucial to use higher voltage levels than that of today's usage to provide the required power for the aircraft propulsion system, especially during the take-off, where at least three times as much power as that in cruise phase is needed.

In this paper, based on the turboelectric N3-X aircraft, a novel architecture for the envisaged all electric N3-X EPS is proposed and discussed, aircraft dimensions are estimated, and potential conductors are selected for cables connecting different buses. In the proposed EPS, power is provided using four EEUs and distributed to fourteen motors through the designed MVDC bipolar ±5 kV distribution system to provide the 25 MW thrust power required for take-off. To analyze the proposed EPS architectures, power flow solvers for DC systems are needed. To this end, this paper develops an accurate methodology using the monotone mapping method for PF for DC power systems. Then, the model is used for the envisaged N3-X EPS aircraft to obtain the power flowing in the system under normal condition and during single contingencies. Finally, using DC power flow models developed, it is shown that the proposed DC EPS can meet requirements under normal condition and single contingencies.

This paper is organized as follows: in section 2, after discussing electrified propulsion architectures, all electric NASA N3-X aircraft EPS is proposed and discussed. In section 3, aircraft dimensions are estimated and discussed in detail. Section 4 aims to select conductors for cables connecting different buses. In the same section, cable lengths are also calculated based on estimated dimensions in section 3, and resistances of selected potential conductors are calculated accordingly. In section 5, the PF problem is formulated and, then, the monotone mapping technique is delineated and modified as the PF solver; and PF results are presented and discussed. Section 6 concludes the most important findings of this paper.

2. ALL ELECTRIC N3-X AIRCRAFT EPS

With today's technologies, it is not possible to provide all power required in a wide-body AEA electrically using EEUs, including batteries, fuel cells (FC), and supercapacitors (SC). Therefore, other electrical propulsion architectures, namely turboelectric and hybrid electric, were introduced and desig-ned as well, and concepts such as NASA N3-X are enjoying these architectures. Possible electrical propulsion architectu-res are shown in Figure 2 [4, 6]. As shown in the figure, in a turboelectric architecture, the power extracted from engines is converted to electrical form and is distributed electrically to motors/fans to provide the required thrust power. Hybrid electric architecture can be either series or parallel, or a combination of both. In a series hybrid architecture, the power extracted from engines is utilized to charge EEUs and provide the thrust power, while in a parallel hybrid architecture, power from EEUs and engines are mounted mechanically to drive motors/fans. In Figure 2, although batteries are considered as EEUs, FCs and SCs can also be found within EEU units. Finally, in an all electric propulsion architecture, engines are completely removed, and only EEUs are responsible for prov-iding power, and the power is indeed distributed electrically to motors/fans to provide the required thrust power.

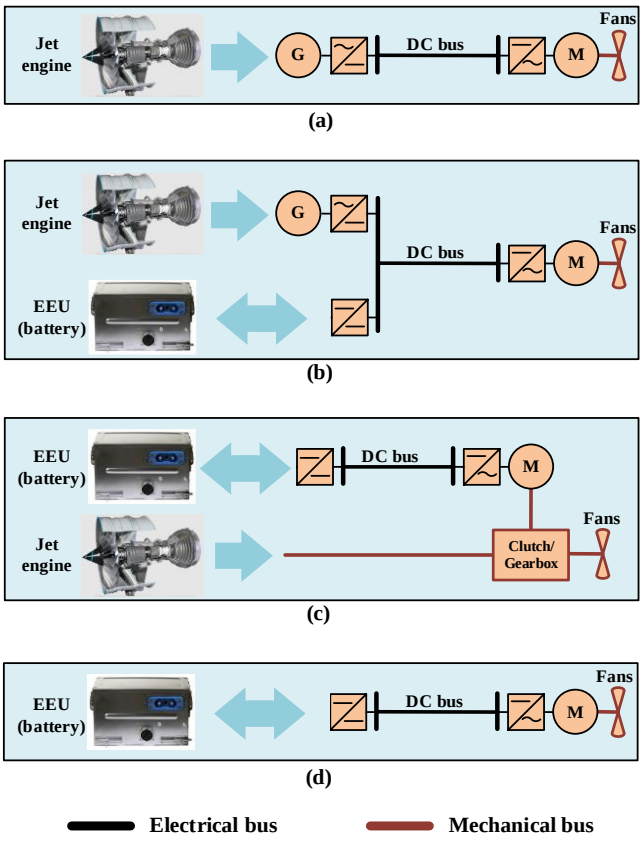

Figure 2. Possible electrical propulsion architectures [6]: (a) turboelectric, (b) series hybrid electric, (c) parallel hybrid electric, and (d) all electric.

Figure 3 shows the all-electric NASA N3-X aircraft EPS proposed in this paper. In addition, Figure 4 shows the propulsion section with more detail. In this architecture, all required thrust power is provided by EEUs including batteries, FCs, and SCs, and distributed electrically to motors. A bipolar ±5 kV_{DC} is considered to supply motors, and a bipolar ±0.5 kV_{DC} is suggested to supply non-propulsive loads, such as a wing-ice protection system (WIPS). Also, a 28 V_{DC} is considered to supply avionics as exactly as that in conventional aircraft and commercialized MEA such as the Boeing 747, the Airbus 380, and the Boeing 787.

The required electrical power in the all-electric N3-X aircraft for take-off is 25 MW which is provided by fourteen distributed fans; each has a capacity of 1.785 MW and is supplied with a voltage level of ±5 kV_{DC}. The capacity of each EEU is considered 25/3=8.34 MW. The architecture shown in Figure 4 is reliable both in normal condition and all n-1 contingency situations even losing a busbar.

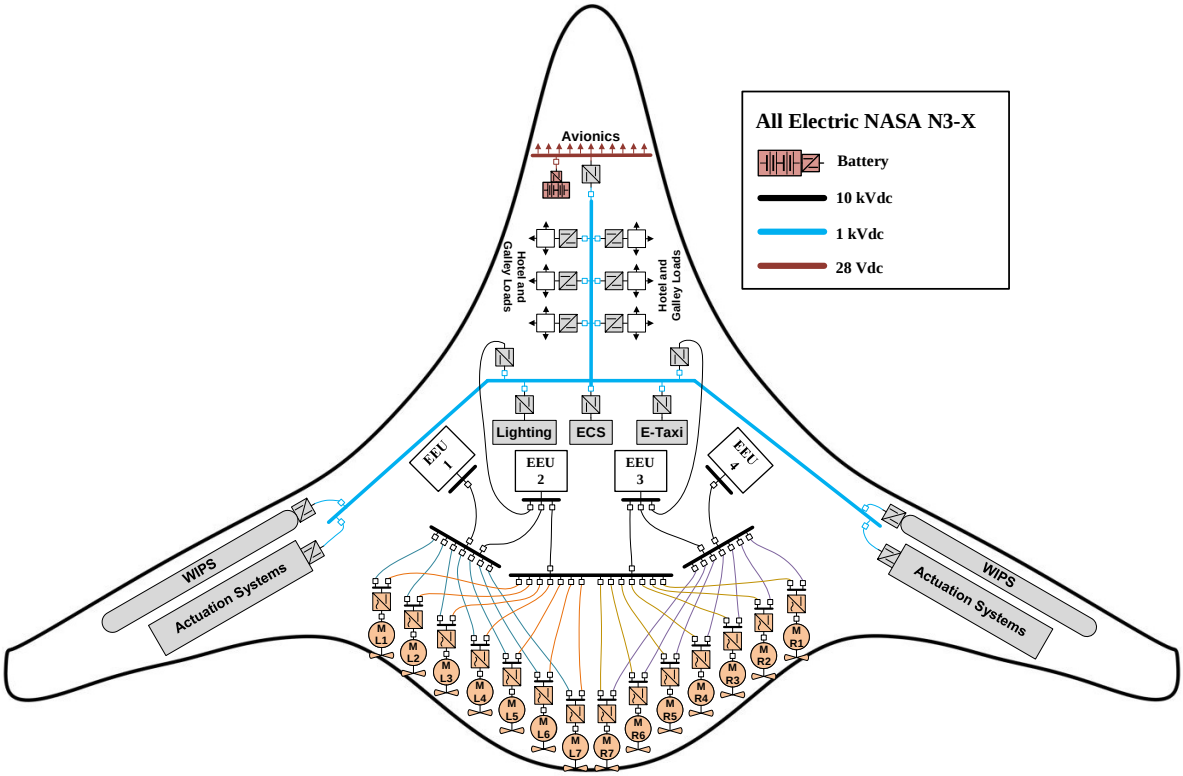

Figure 3. Proposed all electric NASA N3-X aircraft EPS

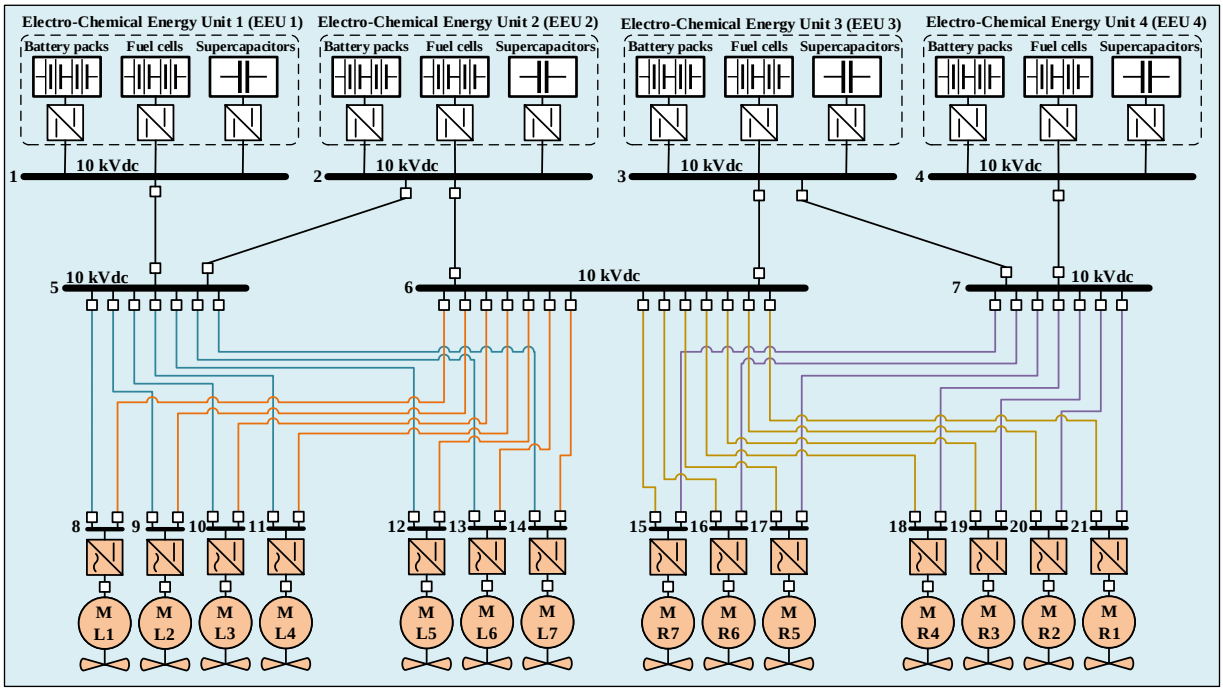

Figure 4. Propulsion section architecture of the proposed all electric NASA N3-X aircraft EPS.

3. ESTIMATION OF AIRCRAFT DIMENSIONS

To the best of the authors' knowledge, there is no document in which NASA N3-X dimensions were presented. However, aircraft dimensions are needed to perform the PF analysis. Using available information from previously designed concepts, this section aims to estimate the dimensions of all-electric N3-X aircraft. The complete estimated dimensions are illustrated in Figure 5. Note that both sides of the aircraft

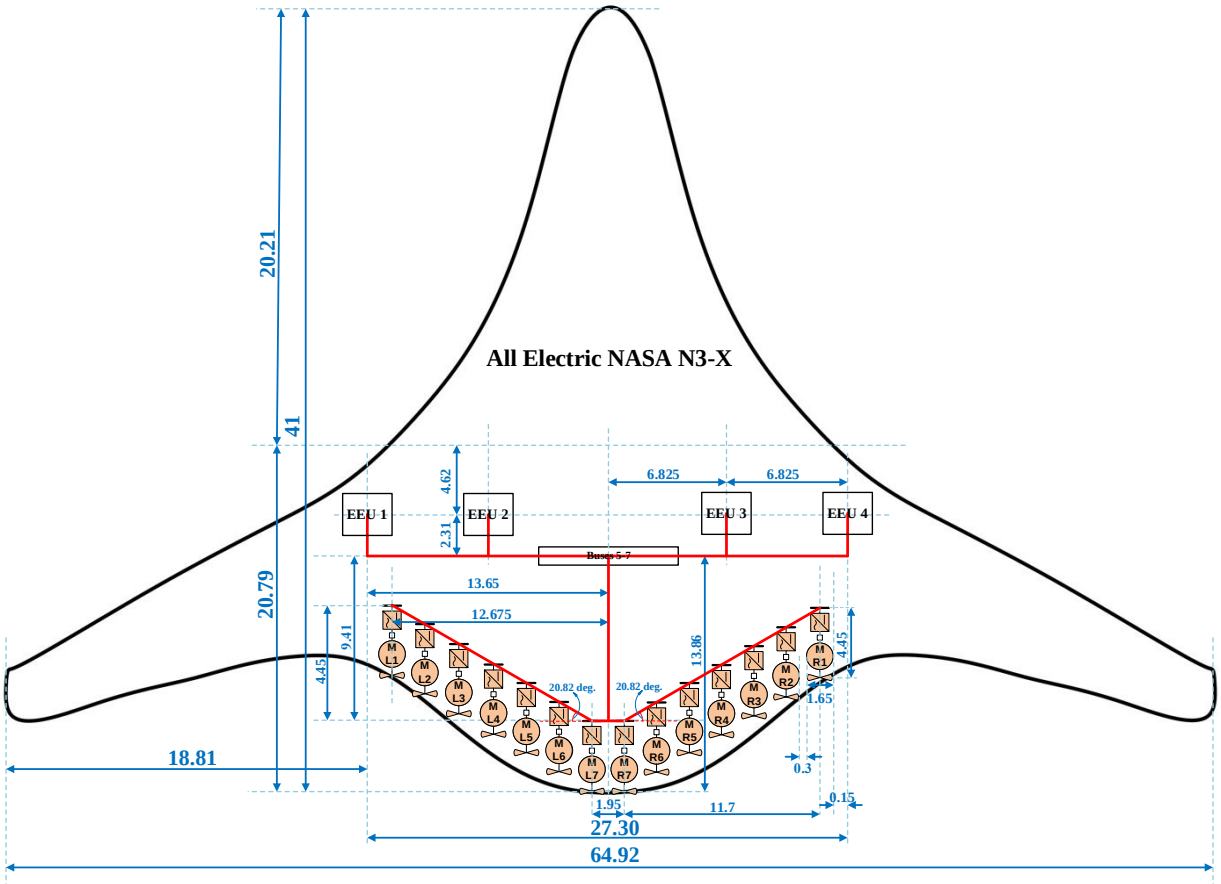

Figure 5. The estimated dimensions of our proposed all electric NASA N3-X aircraft.

are considered identical, and if a number is indicated on one side, it applies to the other side of the aircraft as well.

Based on Cranfield AVD work [9], the aircraft's length, width, and height are inferred as follows: 64.92 m wing-to-wing, 41 m length, and 7 m height which is not indicated in Figure 5. Each wing's length is inferred to be 18.81 m, and the fuselage width is inferred to be 27.30 m. Wings' lengths and fuselage width are estimated using information presented in [10, 11] based on available information about the N+3 H1 study and SAX40 HWB design. The wing length to total wing-to-wing distance (wl/wwd) ratio is kept similar to [10] where $wl/wwd = 0.287$. Here, in the proposed N3-X AEA:

$$wl/wwd = 18.81\ m/(18.81\ m + 27.30\ m + 18.81\ m) = 0.290$$

Also, to find different parts' lengths of the total length of the aircraft (41 m), available information on N2A and N2B concepts are used [12], where it is tried to keep the same proportional lengths. In [12] (p. 30), the total length of the N2A is 1614.1 inch and the tip-to-propulsion-system length to total length of the aircraft ratio is:

$$(539.6\ inch + 232.5\ inch)/1614.1\ inch = 0.48$$

The same ratio is in our proposed all-electric N3-X aircraft:

$$20.21\ m/41\ m = 0.49$$

In addition, the dimensions of each motor are inferred as precisely as that presented in [13]. Therefore, the length and width of each motor are inferred to be 4.45 m and 1.65 m, respectively. It is assumed that motors are not located on the wing; a 0.3 m distance between two adjacent motors is considered. Also, it is assumed that buses 5-7 are placed at one location at the center of wing-to-wing direction and at a distance of 2/3×20.79=13.86 m from the bottom of the aircraft.

An H configuration, shown in Figure 4, is proposed for the main part of EPS. As seen in Figure 5, MR1 and ML1 are 4.45 m closer to the nose of aircraft than MR7 and ML7, and, as a result, motors are distributed with an angle of 20.82°.

4. Conductors' Resistances and Lengths

In this section, resistances of cables connecting different buses are calculated. For cables connecting buses 5-7 to motors (buses 8-21), two final types of conductors are selected, and PF results for both conductors are presented. In selecting conductors, the ratio of $M = I/(d.w)$ is targeted to be maximized, where I is the cable ampacity, d is the outer diameter of the conductor, and w is the total weight of the conductor. Since the PF analysis is done for the steady-state during the take-off phase of the flight, each motor works at its full capacity and consumes 1.785 MW constant power at the

voltage rating ~±5 kV_{DC}. Therefore, the required ampacity for cables connecting motors to buses 5-7 is at least 178.5 A. Among different types of conductors in [14] in the ampacity range obtained above, all aluminum conductors (AAC) conductors lead to a higher amount for M. AAC Iris and AAC Pansy with ampacities of 185 A and 215 A, respectively, are considered for studies. Also, for cables connecting buses 1-4 to buses 5-7, our preliminary analysis shows that a maximum 1 kA ampacity is needed; thus, Helens/AAC/TW, a trapezoidal all-aluminum 1350 concentric-lay-stranded, with the ampacity of 1055 A is selected for the core conductor of the envisaged ±5 kVdc aircraft power cable. The reason to select an AAC/TW conductor is that this type of conductor enjoys the highest M ratio compared to other types of conductors. DC resistance of conductors calculated at 75°C was used for PF analysis.

For the H switchgear configuration proposed in Figure 4, the lengths of cables connecting different buses are indicated in Table 1. To make it clear and as an example, the cable length connecting bus 6 to bus 19 is calculated as below:

$$9.41 + 1.95/2 + (4 \times 1.65 + 4 \times 0.3)/\cos(20.82°) = 18.7299\ m$$

Note that 0.5 m is added to all estimated lengths, and the result is multiplied by 1.1 to cover different uncertainties. Therefore, 18.7299 m is not used to calculate the resistance of the cable connecting bus 6 and bus 19, (18.7299 m+0.5 m)×1.1=21.1529 m is used instead.

Table 1. Lengths and resistances of cables

from (bus)	to (bus)	(length+0.5) × 1.1 (m)	Resistance (Helens/Iris) ($\times 10^{-3}\ \Omega$)	Resistance (Helens/Pansy) ($\times 10^{-3}\ \Omega$)
			Helens	Helens
1	5	18.1060	1.1027	1.1027
2	5, 6	10.5985	0.6454	0.6454
3	6, 7	10.5985	0.6454	0.6454
4	7	18.1060	1.1027	1.1027
			Iris	Pansy
5, 6	8	25.7426	26.7080	21.2197
5, 6	9	23.4477	24.3270	19.3279
5, 6	10	21.1529	21.9461	17.4363
5, 6	11	18.8581	19.5652	15.5447
5, 6	12	16.5633	17.1844	13.6531
5, 6	13	14.2683	14.8034	11.7614
5, 6	14	11.9735	12.4225	9.8698
6, 7	15	11.9735	12.4225	9.8698
6, 7	16	14.2683	14.8034	11.7614
6, 7	17	16.5633	17.1844	13.6531
6, 7	18	18.8581	19.5652	15.5447
6, 7	19	21.1529	21.9461	17.4363
6, 7	20	23.4477	24.3270	19.3279
6, 7	21	25.7426	26.7080	21.2197

5. POWER FLOW ANALYSIS

In this section, PF analysis is done for 1) combination of Helens/AAC/TW for cables connecting buses 1-4 to buses 5-7 and AAC Iris for cables connecting buses 5-7 to buses 8-21, and for 2) Helens/AAC/TW for cables connecting buses 1-4 to buses 5-7 and AAC Pansy for cables connecting buses 5-7 to buses 8-21. Since the target network (all-electric N3-X aircraft EPS shown in Figs. 3 and 4) is a DC network, a PF method is needed for DC networks. The monotone mapping, which was also used in [15], is modified and employed here to solve the PF problem.

PF Problem Formulation for DC Power Systems

Let us introduce the graph $\mathcal{G} = (\mathcal{N}^+, \mathcal{L})$ with N nodes, where nodes ($\mathcal{N}^+ = \{1, \dots, N\}$) represent buses and lines are represented by edges ($\mathcal{L}$). Also, voltage-controlled buses and load buses belong to subsets of $\mathcal{N}^+$ and are $\mathcal{V}$ and $\mathcal{P} := \mathcal{N}^+ \backslash \mathcal{V}$, respectively. This paper uses n_t to refer to all buses, n_V to refer to voltage-controlled buses, and n_L to refer to load buses. For $n \in n_L$ with voltage v_n, current injected from the bus is presented as:

$$i_n = -\frac{p_n^{cst}}{v_n} - i_n^{cst} - y_n^{cst} v_n \tag{1}$$

where p_n^{cst} presents constant-power loads connected to the bus n, and i_n^{cst} and y_n^{cst} present constant-current and constant-admittance loads connected to the bus n, respectively.

Since it is assumed that the aircraft EPS is at steady-state during take-off phase of the flight, only constant-power loads are present and equation (1) can be rewritten as:

$$i_n = -\frac{p_n^{cst}}{v_n} \tag{2}$$

where $p_n^{cst} < 0$ for generation and $p_n^{cst} > 0$ for loads.

Using Kirchhoff's current law, we have:

$$i_n = \sum_{k \in n_t} y_{nk}(v_n - v_k) \tag{3}$$

where y_{nk} is the admittance between buses n and k if they are directly connected.

By defining y_n and k_n as:

$$y_n = \sum_{k \in n_t} y_{nk} \tag{4}$$

$$k_n = \sum_{k \in n_V} y_{nk} v_k \tag{5}$$

and combining equations (2) and (3) and multiplying the result by v_n, it gives:

$$k_n v_n^2 = \sum_{k \in n_L} y_{nk} v_n v_k + k_n v_n - p_n^{cst} \tag{6}$$

Equation (6) is the general form of the PF problem in this paper and should be solved.

Monotone mapping solver

By defining $u_n = v_n^2$ and applying it to equation (6) it gives:

$$u_n = \sum_{k \in n_L} \frac{y_{nk}}{y_n} \sqrt{u_n u_k} + \frac{k_n}{y_n} \sqrt{u_n} - \frac{p_n^{cst}}{y_n} \tag{7}$$

Equation (7) is solved by defining the n_L-length vector $\boldsymbol{u}$ and the mapping $\boldsymbol{f}$, where $\boldsymbol{u} = \boldsymbol{f}(\boldsymbol{u})$ and entries of $\boldsymbol{f}$ are as below:

$$f_n(\boldsymbol{u}) = \sum_{k \in n_L} \frac{y_{nk}}{y_n} \sqrt{u_n u_k} + \frac{k_n}{y_n} \sqrt{u_n} - \frac{p_n^{cst}}{y_n} \qquad (8)$$

Therefore, the PF problem translates into solving iterations of

$$\boldsymbol{u}^{t+1} = \boldsymbol{f}(\boldsymbol{u}^t) \qquad (9)$$

One may wonder whether this iteration converges to the solution. If we define $\underline{u}$ and $\overline{u}$ as the minimum and the maximum values of $\boldsymbol{u}$, since there is no constant-current component in the system shown in Figure 4 (and, as a result, for $\forall n \in n_L$ we get $i_n^{cst} = 0$), equation (10) is surely satisfied for $\forall n \in n_L$:

$$i_n^{cst} \leq \frac{\underline{u}}{\sqrt{2\overline{u} - \underline{u}}} y_n \qquad (10)$$

Also, there is no constant-admittance component in the system shown in Figure 4 (and, as a result, for $\forall n \in n_L$ we get $y_n^{cst} = 0$); also, $p_n^{cst} \geq 0$ for all $n \in n_L$. Therefore, the equation (11) is surely satisfied for $\forall n \in n_L$:

$$\overline{u} y_n^{cst} + \sqrt{\overline{u}} i_n^{cst} + p_n^{cst} \geq 0 \qquad (11)$$

Since both equations (10) and (11) are satisfied for the all electric N3-X aircraft EPS, the solution resulted from iterations in equation (9) would converge to a solution [15].

PF results

Using the PF solver explained in this section, PF problem for the envisaged all electric N3-X aircraft EPS is solved and results for Helens/AAC/TW accompanied by AAC Iris and AAC Pansy conductors are presented and discussed. The aircraft EPS is assumed at steady-state during take-off, where each motor consumes 1.785 MW constant power. The EPS can sustain the flow of power in normal condition and all n-1 contingency situations.

PF analysis results for all electric N3-X aircraft are presented in Tables 2-9. Tables 2 and 3 show PF results in normal condition for Helens/AAC/TW and AAC Iris conductor; PF results in normal condition for Helens/AAC/TW and AAC Pansy are shown in Tables 4 and 5; PF results for Helens/AAC/TW and AAC Iris in case of losing of bus 6 (as an example of losing a busbar) are presented in Tables 6 and 7; and PF results for Helens/AAC/TW and AAC Pansy in case of losing of bus 6 are presented in Tables 8 and 9. As seen from the Tables, the flow of power is sustained to all motors both in normal condition and the considered faulty situation without overloading cables and unacceptable voltage drops. AAC Pansy shows more satisfactory PF results compared to AAC Iris. However, AAC Iris has superiority in terms of outer diameter and weight and enjoys the highest *M* ratio. Therefore, as long as the thermal limit of cables is taken for granted, AAC Iris would be the choice.

Table 2. PF results in normal condition (Helens/Iris)

bus no.	1,2,3,4	5	6	7	8	9
V (kV)	5.0000	4.9999	4.9998	4.9999	4.9986	4.9988
bus no.	10	11	12	13	14	15
V (kV)	4.9989	4.9990	4.9991	4.9992	4.9993	4.9993
bus no.	16	17	18	19	20	21
V (kV)	4.9992	4.9991	4.9990	4.9989	4.9988	4.9986

Table 3. PF results in normal condition (Helens/Iris)

bus no.		Current (A)	bus no.		Current (A)
from	to		from	to	
1	5	239.46	6	12	85.66
2	5	409.08	6	13	85.08
2	6	601.22	6	14	84.27
3	6	601.22	6	15	84.27
3	7	409.08	6	16	85.08
4	7	239.46	6	17	85.66
5	8	91.60	6	18	86.10
5	9	91.82	6	19	86.44
5	10	92.10	6	20	86.72
5	11	92.44	6	21	86.95
5	12	92.88	7	15	94.25
5	13	93.45	7	16	93.45
5	14	94.25	7	17	92.88
6	8	86.95	7	18	92.44
6	9	86.72	7	19	92.10
6	10	86.44	7	20	91.82
6	11	86.10	7	21	91.60

Table 4. PF results when bus 6 is lost (Helens/Iris)

bus no.	1,2,3,4	5	6	7	8	9
V (kV)	5.0000	4.9997	-	4.9997	4.9974	4.9976
bus no.	10	11	12	13	14	15
V (kV)	4.9978	4.9980	4.9982	4.9984	4.9986	4.9986
bus no.	16	17	18	19	20	21
V (kV)	4.9984	4.9982	4.9980	4.9978	4.9976	4.9974

Table 5. PF results when bus 6 is lost (Helens/Iris)

bus no.		Current (A)	bus no.		Current (A)
from	to		from	to	
1	5	461.53	6	12	-
2	5	788.47	6	13	-
2	6	-	6	14	-
3	6	-	6	15	-
3	7	788.47	6	16	-
4	7	461.53	6	17	-
5	8	178.59	6	18	-
5	9	178.59	6	19	-
5	10	178.58	6	20	-
5	11	178.57	6	21	-
5	12	178.56	7	15	178.55
5	13	178.56	7	16	178.56
5	14	178.55	7	17	178.56
6	8	-	7	18	178.57
6	9	-	7	19	178.58
6	10	-	7	20	178.59
6	11	-	7	21	178.59

Table 6. PF results in normal condition (Helens/Pansy)

bus no.	1,2,3,4	5	6	7	8	9
V (kV)	5.0000	4.9999	4.9998	4.9999	4.9989	4.9990
bus no.	10	11	12	13	14	15
V (kV)	4.9991	4.9991	4.9992	4.9993	4.9994	4.9994
bus no.	16	17	18	19	20	21
V (kV)	4.9993	4.9992	4.9991	4.9991	4.9990	4.9989

Table 7. PF results in normal condition (Helens/Pansy)

bus no.		Current (A)	bus no.		Current (A)
from	to		from	to	
1	5	241.25	6	12	84.91
2	5	412.14	6	13	84.21
2	6	596.32	6	14	83.24
3	6	596.32	6	15	83.24
3	7	412.14	6	16	84.21
4	7	241.25	6	17	84.91
5	8	92.07	6	18	85.44
5	9	92.34	6	19	85.86
5	10	92.68	6	20	86.19
5	11	93.09	6	21	86.47

5	12	93.62	7	15	95.28
5	13	94.32	7	16	94.32
5	14	95.28	7	17	93.62
6	8	86.47	7	18	93.09
6	9	86.19	7	19	92.68
6	10	85.86	7	20	92.34
6	11	85.44	7	21	92.07

Table 8. PF results when bus 6 is lost (Helens/Pansy)

bus no.	1,2,3,4	5	6	7	8	9
V (kV)	5.0000	4.9997	-	4.9997	4.9979	4.9980
bus no.	10	11	12	13	14	15
V (kV)	4.9982	4.9984	4.9985	4.9987	4.9989	4.9989
bus no.	16	17	18	19	20	21
V (kV)	4.9987	4.9985	4.9984	4.9982	4.9980	4.9979

Table 9. PF results when bus 6 is lost (Helens/Pansy)

bus no.		Current (A)	bus no.		Current (A)
from	to		from	to	
1	5	461.50	6	12	-
2	5	788.41	6	13	-
2	6	-	6	14	-
3	6	-	6	15	-
3	7	788.41	6	16	-
4	7	461.50	6	17	-
5	8	178.58	6	18	-
5	9	178.57	6	19	-
5	10	178.56	6	20	-
5	11	178.56	6	21	-
5	12	178.55	7	15	178.54
5	13	178.55	7	16	178.55
5	14	178.54	7	17	178.55
6	8	-	7	18	178.56
6	9	-	7	19	178.56
6	10	-	7	20	178.57
6	11	-	7	21	178.58

In this paper, PF analysis was done by considering all EEU buses as voltage-controlled buses and, equivalently, variable power generators. Indeed, this assumption resulted in the least loss of power, which was 4.28 kW. For this assumption, the generated power of EEU1-4 was ~2.4 MW, 10 MW, 10 MW, and 2.4 MW, respectively, under normal conditions for the Helens/Pansy conductors described above. Therefore, we should consider different capacities for EEUs. Another paper [16] assumed that buses 2 and 3 were constant power generators. EEU2 and EEU3 are sized to have a capacity of ~8.3 MW (25 MW/3). EEU2 and EEU3 were set to work at 80% of their capacity (6.664 MW) as long as all EEUs supplied the EPS. Also, EEU2 and EEU3 were assumed to work at 100% of their capacity (8.3 MW) if a failure led to losing an EEU. Since the architecture is split into two separate architectures when bus 6 is lost, bus 1 and bus 4 are both considered voltage-controlled buses. Therefore, buses 1 and 4 both provide the power loss in the EPS, and if, for example, EEU1 fails, bus 4 would work as the only voltage-controlled bus and provide the power loss, and vice versa. Besides the EPS architecture presented in this paper, Figure 4, two other EPS architectures for all-electric N3-X aircraft were also introduced in [17]. A comprehensive study of the studies presented in this paper and [16, 17] was presented in [18].

6. Conclusion

In this paper, the NASA turboelectric aircraft is fully electrified, and a new switchgear configuration for the envisaged all electric N3-X aircraft EPS is proposed and analyzed. In the proposed EPS architecture, 25 MW electrical power required during take-off is provided using four electrochemical energy units (EEU), including batteries, fuel cells (FC), and supercapacitors (SC); and distributed through a ±5 kV H switchgear configuration to fourteen distributed motors, each of which has the capacity of 1.785 MW. Helens/AAC/TW conductor is selected for cables connecting EEUs to busbars, and authors conclude that cables connecting motors to busbars should be either AAC Iris or AAC Pansy. A PF solver for DC power systems based on monotone mapping is developed. PF results for the take-off phase which needs the most loads show that the designed EPS can sustain the flow of power both in normal condition as well as all n-1 contingency situations.

Acknowledgment

The work presented herein was funded in part by the Advanced Research Projects Agency-Energy (ARPA-E), U.S. Department of Energy, under Award Number DE-AR0001465. The views and opinions of authors expressed herein do not necessarily state or reflect those of the United States Government or any agency thereof.

References

[1] P. J. Ansell and K. S. Haran, "Electrified airplanes: A path to zero-emission air travel," *IEEE Electrific. Mag.*, vol. 8, no. 2, pp. 18-26, 2020.

[2] A. Barzkar and M. Ghassemi, "Electric power systems in more and all electric aircraft: A review," *IEEE Access*, vol. 8, pp. 169314-169332, 2020.

[3] B. Sarlioglu and C. T. Morris, "More electric aircraft: Review, challenges, and opportunities for commercial transport aircraft," *IEEE Trans. Transport. Electrific.*, vol. 1, no. 1, pp. 54-64, 2015.

[4] *Commercial aircraft propulsion and energy systems research: Reducing global carbon emissions*. National Academies Press, 2016.

[5] M. J. Armstrong *et al.*, "Architecture, voltage and components for a turboelectric distributed propulsion electric grid," *NASA Technol. Report Server (NTRS)*, 2015.

[6] A. Barzkar and M. Ghassemi, "Components of electric power systems in more and all electric aircraft: A review identifying challenges and future research needs," submitted, 2021.

[7] R. Jansen, C. Bowman, and A. Jankovsky, "Sizing power components of an electrically driven tail cone thruster and a range extender," in *16th AIAA Aviation Technol. Integ. Ops. Conf.*, 2016, p. 3766.

[8] M. J. Armstrong, C. A. Ross, M. J. Blackwelder, and K. Rajashekara, "Trade studies for NASA N3-X

turboelectric distributed propulsion system electrical power system architecture," *SAE Int. J. Aerosp.*, vol. 5, no. 2012-01-2163, pp. 325-336, 2012.
[9] https://www.youtube.com/watch?v=0_50FcUgUf8
[10] J. Kim, K. Kwon, S. Roy, E. Garcia, and D. N. Mavris, "Megawatt-class turboelectric distributed propulsion, power, and thermal systems for aircraft," in *AIAA Aerosp. Sci. Meeting*, 2018, p. 2024.
[11] J. Hileman, Z. Spakovszky, M. Drela, M. Sargeant, and A. Jones, "Airframe design for silent fuel-efficient aircraft," *J. Aircraft*, vol. 47, no. 3, pp. 956-969, 2010.
[12] R. T. Kawai, "Acoustic prediction methodology and test validation for an efficient low-noise hybrid wing body subsonic transport," 2011.
[13] H. D. Kim, J. L. Felder, M. T. Tong, J. J. Berton, and W. J. Haller, "Turboelectric distributed propulsion benefits on the N3-X vehicle," *Aircraft Eng. Aerosp. Tech. Int. J.*, 2014.
[14] "Electric Utility U.S. Energy Products for Power Generation, Transmission & Distribution" General Cable, May 2017.
[15] S. Taheri and V. Kekatos, "Power flow solvers for direct current networks," *IEEE Trans. Smart Grid*, vol. 11, no. 1, pp. 634-643, 2019.
[16] M. Ghassemi and A. Barzkar, "Power flow solvers for medium voltage direct current (MVDC) microgrids," *The 6th IEEE Workshop on the Electronic Grid (eGrid 2021)*, Virtual, November 8-10, 2021.
[17] M. Ghassemi and M. Saghafi, "Optimal electric power system architectures for wide body all electric aircraft," *The 43rd IEEE Aerospace Conference*, Big Sky, Montana, March 5-12, 2022.
[18] M. Ghassemi, A. Barzkar, and M. Saghafi "All-electric NASA N3-X aircraft electric power systems," 2021, submitted.

BIOGRAPHY

Mona Ghassemi *(Senior Member, IEEE) received her B.Sc. degree from Shahed University, Tehran, Iran in 2004, and M.Sc. and Ph.D. degrees (Hons.) from the University of Tehran, Tehran, Iran in 2007 and 2012, respectively, all in electrical engineering. She spent two years (2013–2015) researching as a Postdoctoral Fellow at NSERC/Hydro-Quebec/UQAC Industrial Chair on Atmospheric Icing of Power Network Equipment (CIGELE) at the University of Québec at Chicoutimi (UQAC). She was also a Postdoctoral Fellow at the Electrical Insulation Research Center, Institute of Materials Science, University of Connecticut, Storrs, CT, USA, from 2015 to 2017. In 2017, she joined the Department of Electrical and Computer Engineering, Virginia Tech, Blacksburg, VA, USA, as an Assistant Professor, and since 2021, she has been named as both the Steven O. Lane Junior Faculty Fellow and the College of Engineering Faculty Fellow. She has been a registered Professional Engineer in the Province of Ontario, Canada, since 2015. Dr. Ghassemi is an At-Large Member of the Administrative Committee of the IEEE Dielectrics and Electrical Insulation Society (DEIS) from 2020 to 2023, a Corresponding Member of the IEEE Conference Publication Committee of the IEEE Power and Energy Society (PES), Active Member of several CIGRE working groups and IEEE Task Forces, and a Member of the Education Committee of the IEEE DEIS and PES. She is a recipient of the 2021 Department of Energy (DOE) Early Career Research Program Award, the 2020 National Science Foundation (NSF) CAREER Award, and the 2020 Air Force Office of Scientific Research (AFOSR) Young Investigator Research Program (YIP) Award. She is Associate Editor of IEEE Transactions on Dielectrics and Electrical Insulation, IEEE Transactions on Industry Applications, High Voltage, International Journal of Electrical Engineering Education, Power Electronic Devices and Components (Elsevier), and a Guest Editor for Energies. She also received the 2020 Contribution Award from the High Voltage journal. Her research interests include electrical insulation materials and systems, high-voltage/field technology, Multiphysics modeling, electromagnetic transients in power systems, and power system analysis and modeling.*

Ashkan Barzkar *(Student Member, IEEE) received his B.Sc. degree from the University of Tehran, Tehran, Iran, in 2017, and his M.Sc. degree from Sharif University of Technology, Tehran, Iran, in 2020, both in electrical engineering. He is currently pursuing his studies towards a Ph.D. degree in electrical engineering at Virginia Tech, Blacksburg, VA, USA. His research interests include electric power systems, transportation electrification, and power electronics.*